PCCP

Accepted Manuscript

ROYAL SOCIETY OF CHEMISTRY

www.rsc.org/pccp

Theoretical Investigation on the Mechanism and Dynamics of Oxo Exchange of Neptunyl(VI) Hydroxide in Aqueous Solution

Xia Yang[a,*], Zhifang Chai[a,b], Dongqi Wang[a,*]

[a]CAS Key Laboratory of Nuclear Radiation and Nuclear Energy Techniques, and Multidisciplinary Initiative Center, Institute of High Energy Physics, Chinese Academy of Sciences, Beijing 100049, China

[b]School of Radiation Medicine and Interdisciplinary Sciences (RAD-X), Soochow University, Suzhou 215123, China

E-mail: dwang@ihep.ac.cn

yangxia@ihep.ac.cn

Abstract

Four types of reaction mechanisms for the oxo ligand exchange of monomeric and dimeric neptunyl(VI) hydroxide in aqueous solution were explored computationally with density functional theory (DFT) and ab initio classical molecular dynamics. The obtained results were compared with previous studies on the oxo exchange of uranyl hydroxide, as well as with experiments. It is found that the stable T-shape $[NpO_3(OH)_3]^{3-}$ intermediate is a key species for oxo exchange in the proton transfer of mononuclear Path I and binuclear Path IV, similar to the case of uranyl(VI) hydroxide. Path I is thought as a preferred oxo exchange mechanism of neptunyl(VI) hydroxide in our calculations, due to the lower activation energy (22.7 and 13.1 kcal/mol for $\Delta G^{\ddagger}$ and $\Delta H^{\ddagger}$, respectively) for the overall reaction. Path II via a cis-neptunyl structure assisted by a water molecule might be a competitive channel against the Path I in mononuclear mechanism, owing to a rapid dynamical process occurring on Path II. In binuclear mechanism Path IV, oxo exchange is accomplished via the interaction between $[NpO_2(OH)_4]^{2-}$ and T-shape $[NpO_3(OH)_3]^{3-}$ with the low activation energy for the rate-determining step, however, the overall energy required to fulfill the reaction is slightly higher than that in mononuclear Path I, suggesting a possible binuclear process at higher energy region. The chemical bonding evolution along the reaction pathways was discussed by using topological methodologies of the electron localization function (ELF).

Keywords: Neptunyl(VI) hydroxide, mechanism, dynamics, oxo exchange, DFT calculation, ELF analysis.

1. Introduction

Experimental and theoretical investigations of ligand exchange/substitution reactions on linear actinyl ions in aqueous environment are active fields due to their relevance to environmental safety and reprocessing of spent nuclear fuel. Of particular interests in actinyl chemistry is the oxo ligand (so-called “yl”-oxygen) exchange for

further actinyl functionalization. The exchange of the "yl"-oxygen in actinyl ion is expected to be pH dependent[1, 2] and has been a subject of controversy over decades.

A facile exchange between the oxo ligands at equatorial and axial positions has been experimentally observed for uranyl under highly alkaline conditions but not in acidic $HClO_4$ solution, suggesting the importance of a basic environment[3]. This process was likely relevant to a dynamic equilibrium between tetra- and penta-coordination in the equatorial plane, according to the equation: $[UO_2(OH)_4]^{2-}_{(aq)}+OH^-_{(aq)} \leftrightarrow [UO_2(OH)_5]^{3-}_{(aq)}$. In addition, a rather low activation energy ($\Delta H^{\neq}$ = 9.8 ± 0.7 kcal/mol) is highly unusual because it is far from enough to break the strong triple uranyl bond. This unique phenomenon has invoked extensive experimental and theoretical studies to understand the complexation of uranyl ion with hydroxide[4-20], among which some studies[9, 12-17] suggested that uranyl tetrahydroxide is more favorable energetically than the pentahydroxide in highly alkaline solutions. Recently there has been substantial effort on the speciation and mechanisms of oxo exchange, involving monomeric or polymeric hydroxide species composed of one or more uranyl moieties under acidic or alkaline conditions [7-11, 19-25].

Up to date, although there is no direct evidence experimentally to validate proposed mechanisms, among monomeric mechanisms, a plausible mechanism proposed by Shamov and Schreckenbach[9] appears to be a satisfactory explanation of the experimental observations, and which was independent of methods, suggesting the feasibility for "yl-"oxygen of uranyl to exchange with water. A $[UO_3(OH)_3]^{3-}$ intermediate which retains a linear uranyl unit throughout the process, different from the previous *cis*-uranyl intermediate[13, 18, 26], was formed to facilitate the exchange process. According to this mechanism, the first step addresses the experimentally observed coordination equilibrium between $[UO_2(OH)_4]^{2-}$ (aq) and $[UO_2(OH)_5]^{2-}$ (aq) with the presence of hydroxide. The elimination of a water molecule from the pentahydroxide uranyl species then affords the formation of the key $[UO_3(OH)_3]^{3-}$ intermediate, and the proton shuttling from the equatorial hydroxide to the axial oxo group fulfils the oxo ligand exchange. The calculated activation energy of 12.5 kcal/mol to the first step, which is also the rate-limiting step, agrees reasonably with

the experimental value of 9.8 kcal/mol[3, 9]. In addition to this, some experiments [10, 25] suggested that the oxo exchange in alkaline solution could take place via formation of a binuclear complex, which has been computationally identified by a combined experimental and theoretical study[20]. In their studies, both the presence of T-shape $[UO_3(OH)_3]^{3-}$ and the intramolecular proton transfer pathway through a binuclear species $[UO_2(OH)_4^{2-}\bullet UO_3(OH)_3^{3-}]$ were put forward.

Very recently, Clark et al.[27] experimentally studied the "yl"−oxygen exchange in the neptunyl(VI) unit under strong alkaline condition and observed similar phenomena to that of uranyl(VI), i.e. there is a facile oxygen exchange between the neptunyl(VI) and the water solvent, and the EXAFS and Raman data suggests that $[NpO_2(OH_4)]^{2-}$ is the dominant solution species. The activation energy was not measured in experiments. A possible equatorial coordination equilibrium between tetrahydroxide and pentahydroxide neptunyl analogous to uranyl(VI) hydroxide was tentatively proposed while details on the possible species and mechanisms involved in the exchange of "yl"−oxygen of neptunyl(VI) was not provided. This motivated the present theoretical investigation on the oxo ligand exchange mechanism of neptunyl(VI) hydroxide.

In the present work, three possible mechanisms for the axial-equatorial oxygen exchange of monomeric neptunyl(VI) hydroxide, analogous to that of the uranyl(VI) cation within highly alkaline solutions proposed by Shamov and Schreckenbach[9], as well as a dimer scenario similar to that proposed by Moll and Tsushima et al[20], were investigated as following:

(1) *Path I* via a T-shape $[NpO_3]$ pathway: In this mechanism, neptunyl hydroxide with its equatorial positions tetra-coordinated may convert to the penta-coordination mode (eq.1) followed by a water elimination step to yield a T-shape $[NpO_3]$ intermediate, and then the oxo ligand exchange is accomplished by proton shuttling in $[NpO_3(OH)_3]^{3-}$ intermediate with the assistance of water molecule:

$$[NpO_2(OH)_4]^{2-}_{(aq)} + OH^-_{(aq)} \leftrightarrow [NpO_2(OH)_5]^{3-}_{(aq)} \quad (1)$$

$$[NpO_2(OH)_5]^{3-}_{(aq)} \rightarrow [NpO_3(OH)_3]^{3-}_{(aq)} + H_2O_{(aq)} \quad (2)$$

$$[O=Np=O^*(O)(OH)_3\cdot H_2O]^{3-}_{(aq)} \leftrightarrow [O=Np=O(O)(O^*H)(OH)_2\cdot H_2O]^{3-}_{(aq)} \quad (3)$$

(2) *Path II* via a *cis*-[NpO_2] pathway assisted by a water molecule: oxo ligand exchange occurs via a bent *cis*-neptunyl transition state, through proton shuttling with the participance of a water molecule:

$$[O=Np=O^*(OH)_4\cdot H_2O]^{2-} \rightarrow \ cis\text{-}[NpO_2(O^*H)(OH)_3\cdot H_2O]^{2-} \qquad (4)$$

(3) *Path III* via intramolecular proton transfer in the absence of water: in Path III, a stepwise (III_A) or a concerted (III_B) migration of two protons in $[NpO_2(OH)_4]^{2-}$ leads to the occurrence of axial-equatorial oxygen exchange:

$$\text{III\_A:} \qquad [O=Np=O^*(OH)_4]^{2-} \rightarrow \ cis\text{-}[NpO_2(O^*H)(OH)_3]^{2-} \qquad (5)$$

$$\text{III\_B:} \qquad [^*O=Np=O^*(OH)_4]^{2-} \rightarrow \ [NpO_2(O^*H)_2(OH)_2]^{2-} \qquad (6)$$

(4) *Path IV* via intramolecular proton transfer in a binuclear species: in this pathway, the rate-dominating step is proton transfer between the oxygen atoms in a dimeric complex $[NpO_3(OH)_2^{2-}\bullet NpO_3(OH)_3^{3-}]$ formed by the hydrolysis and structural reorganization of the complex $[NpO_2(OH)_4^{2-}\bullet NpO_3(OH)_3^{3-}]$:

$$[O=Np=O^*(O)(OH)_2^{2-}\bullet NpO_3(OH)_3^{3-}] \rightarrow [NpO_3(O^*H)\ (OH)_2^{3-}\bullet NpO_3(OH)_2^{2-}] \qquad (7)$$

where the "*" labels the O^{yl} atom to be exchanged.

The aim of the current study is to provide a systematic investigation on the possible oxo ligand exchange mechanisms in the case of neptunyl(VI) hydroxide with solvent effects taken into account, and a comparison with experiment as well as theoretical mechanisms on uranyl, to comprehend the O^{yl} exchange of actinyl in terms of activation energy and/or the bonding processes for both closed-shell uranyl and open-shell neptunyl ions.

2. Computational Methods

All quantum chemical calculations were performed within the framework of DFT [28] using the hybrid B3LYP functional[29, 30] and the Stuttgart small-core relativistic effective core potential (RECP) and associated valence basis sets for neptunium atom. The geometry optimization of actinide complexes using single-determinant DFT is shown to be generally able to provide reasonable results[31-38]. The Stuttgart small-core RECP treats the 60 electrons in the inner core shells of the neptunium with pseudopotentials, and the valence shells by a segmented contraction scheme of

(14s13p10d8f6g)/[10s9p5d4f3g][39, 40]. The split-valence-shell Gaussian basis sets, 6-311++G(d,p)[41], were employed to handle O and H atoms in full optimization and frequency calculations. This combination is denoted as BS1 here. The B3LYP/BS1 level of calculations have been shown to be able to give results close to the experimental values in many studies of actinide reactions[9, 11, 20, 42, 43].

The electronic configuration of Np(VI) in its doublet state was adopted, corresponding to its lowest-energy spin state. Calculations were carried out using spin-unrestricted methods. No appreciable spin contamination was found in all studied species, with the value of $<S^2>$ between 0.75 and 0.76. Polarizable Continuum Model (PCM)[44] was utilized to evaluate the solvent effect in order to get a better estimate of the possible activation energies, which may be influenced by the solvent environment. All of the targeted structures were fully optimized without symmetry restrictions in aqueous phase, and the nature of optimized structures was characterized by vibrational analysis to be either local minima or saddle point on the potential energy surface. The transition states were verified to possess an imaginary harmonic vibrational frequency that describes the mode of the reaction vector across the energy barrier. Intrinsic reaction coordinate (IRC) calculations[45, 46] in the solution were then carried out to confirm the reactants and products for a given transition state. The corresponding zero-point vibrational energy (ZPVE) and entropy corrections at room temperature were obtained. All energies reported include ZPVE correction. Single-point energy calculations were then carried out to refine energies at MP2 level with a larger basis set aug-CC-pVTZ to describe the non-metal atoms. This composite basis set is labeled as BS2. Note that in the present work, spin-orbit coupling effects were not included. These calculations were carried out with the Gaussian 09 package[47].

The Born−Oppenheimer molecular dynamics (BOMD) method[48, 49] implemented at B3LYP level was applied to simulate the kinetic process of reactions, which uses a fifth-order polynomial fitted to the energy, gradient, and Hessian at each time step. The Hessians are updated for five steps before being recalculated analytically. The rotation sampling temperature was 300 K. A step size of 0.25 $amu^{1/2}$bohr was used for

integrating the trajectories.

The bonding characteristics of all key minima and transition states were studied within the framework of topological methodologies. In particular, the electron localization function (ELF)[50, 51] was utilized to evaluate the bonding evolution along the reaction pathway by the Multiwfn package[52]. For comparison, bonding description based on Mayer bond order[53] and Wiberg bond index[54] was also explored.

3. Results and Discussion

3.1 Path I via a T-shape [NpO_3] pathway. *Structures and Energetics.* Scheme 1 illustrates the 'yl-'oxygen exchange of mononuclear neptunyl hydroxide via a T-shape [NpO_3] pathway. Figure 1 plots the relative free energy profile for Path I, where all located stationary points in aqueous phase, including minima and transition states (TS), are presented. The optimized geometrical parameters of all species and activation enthalpies and Gibbs free energies for the forward (F) and backward (B) processes of Path I in the aqueous phase are tabulated in Table 1 and Table 2, respectively. The frequencies corresponding to the symmetric and antisymmetric neptunyl stretching modes for all species and the imaginary mode for each transition state are also given in Table 1. The geometry of the initial complex 1 ($[NpO_2(OH)_4]^{2-}$) is in good agreement with experimentally determined structure data in solution using EXAFS[27].

Similar to oxo exchange of monomeric uranyl hydroxide[9], Path I begins with neptunyl tetrahydroxide as the starting point and forms a penta-coordinated neptunyl hydroxide intermediate via TS(1,2) at the first step in the alkaline solution. The activation barrier height of this process is 22.7 and 13.1 kcal/mol, corresponding to $\Delta G^{\ddagger}$ and $\Delta H^{\ddagger}$, respectively, comparable to that of uranyl hydroxide (21.3 and 12.5 kcal/mol for $\Delta G^{\ddagger}$ and $\Delta H^{\ddagger}$, respectively in Table 2). However, this penta-coordinated neptunyl hydroxide intermediate 2 is unstable due to the low free energy barrier of 0.9 kcal/mol to the proton transfer between two hydroxide ions (2→3), leading to the appearance of a T-shape [NpO_3] group with two short axial Np=O bonds and a longer equatorial Np-O bond (1.86 and 2.02 Å for axial and equatorial bonds, respectively),

i.e. the formation of the stable intermediate 3. Comparison of the structures of these three isomers (1, 2 and 3 in Table 1) shows that the linear conformation of O=Np=O moiety deforms in 2 and 3 with a bond angle of c.a. 176°.

The intermediate 3 may subsequently pass through two pathways to accomplish the oxo ligand exchange. One involves an intramolecular proton shuttling between axial and equatorial oxygen atoms via TS(3,3*) with a high activation barrier of 29.3 kcal/mol ($\Delta G^{\ddagger F}$). Another pathway evolves via an intermolecular proton transfer with the assistance of a H_2O molecule, i.e. a proton is shifted from H_2O to the oxo group of neptunyl to form intermediate 5 with a lower free energy barrier of 12.4 kcal/mol compared to the former pathway. The intermediate 5 sits on a shallow potential energy surface, which can result in a rapid equilibrium for oxo ligand exchange occurring in the process 4→4* once this favorable activation energy is reached. This suggests a stepwise proton migration, which is different from the mechanism involving a concerted proton transfer proposed previously in the case of oxo exchange of uranyl hydroxide [9]. Note that an intermediate similar to this transient intermediate 5 was also reported in a Car-Parrinello molecular dynamics (CPMD) simulation of oxo exchange of uranyl hydroxide[7] while eluded from previous static DFT calculations for that of uranyl[9].

In the meantime, it can be also noted that in Path I there is a good inverse correlation existing between bond lengths of neptunyl and stretching vibrational frequencies, i.e. with the increase in bond lengths there is a decrease in both symmetric and antisymmetric stretching frequencies going from reactant to products, cf. Table 1.

In summary, Path I is similar to the mechanism proposed in the case of mononuclear uranyl hydroxide[9], with a low barrier to the equilibrium between tetra-hydroxide and penta-hydroxide ($[NpO_2(OH)_4]^{2-}$/$[NpO_2(OH)_5]^{3-}$). However, $[NpO_2(OH)_5]^{3-}$ is a transient intermediate due to very low forward and backward barriers to $[NpO_2(OH)_4]^{2-}$ and T-shape $[NpO_3(OH)_3]^{3-}$ respectively, and once T-shape $[NpO_3]$ intermediate is formed, it is facile to fulfill the "yl"-oxygen exchange by the intermolecular proton transfer. In addition, singlet point calculations by MP2 level

can arrive at the consistent conclusion.

Bonding Evolution Analysis. The ELF and bond order are analyzed to further understand the bonding evolution. ELF shaded surface map with projection and contour line map for the minima and TSs on the Path I are illustrated in Figure 2 for the facile oxo exchange step 4→4* and in supplementary information (ESI, Figure S1) for the step 1→3*. It can be seen that ELF analysis reflects the track of reaction pathway distinctly. Table 3 listed the valence basin population analysis with larger bond alteration and the bond orders represented by both Mayer bond order and Wiberg bond index for all species in Path I.

The ELF topological analysis of the initial complex $[NpO_2(OH)_4]^{2-}$ indicates that there is less covalency between neptunium and hydroxide ion relative to Np-O^{yl} bonds, as evidenced by the weakening of a disynaptic basin V(Np,O) which characterizes a two-center bond; while Np-O^{yl} bond in the neptunyl exhibits a strong disynaptic valence basin with electron pair localization in the bonding region, i.e. both V(Np,O2) and V(Np,O3) are 1.90e. The tendency of the valence basin population analysis is fully consistent with that of bond orders, cf. Table 3.

In the reaction 1→3, T-shape $[NpO_3]$ moiety occurred arising from the newly formed equatorial Np-O7 bond, in which V(Np,O7) shows the main alteration from 1.23e to 1.71e with the corresponding Mayer/Wiberg bond order from 0.57/1.17 to 0.95/2.18 (see Table 3). The ELF topological analysis of TS(3,3*) indicates that O5-H bond breaking and proton shift simultaneously take place at this stage, as evidenced by a trisynaptic V(O5,H,O2) basin as a replacement for the V(O5,H) basin (Figure S1). Meanwhile, V(Np,O5) gradually increases from 1.22e to 1.79e in the process 3→3*, cf. Table 3.

In the case of the step 4→4*, ELF analysis shown in Figure 2 gives a manifest description on axial-equatorial oxygen exchange. The formation of TS(4,5) involves large change of the valence basin population of a water molecule, in which the lack of V(O9,H) disynaptic valence basin is an indication of the broken of the O9-H bond at this step, accompanying with an increasing disynaptic V(O2,H) basin (Figure 2). The ELF of intermediate 5 definitely exhibits the transfer of proton from water to oxo

ligand of neptunyl with the weakened V(Np,O2) basin population and the strengthened disynaptic V(Np,O5) valence basin.

Similar to TS(4,5), the ELF analysis of TS(5,4*) shows that valence basin of O5-H bond is weakened, giving rise to an enhancement of V(O9,H) basin. Meanwhile, V(Np,O2) valence basin is fading, giving place to the formation of the disynaptic V(Np,O5) valence basin. At last, the structure 4* realized the oxo ligand exchange, as evidenced by the existence of the disynaptic V(Np,O5) and V(O2,H) valence basins, taking the place of the disynaptic V(Np,O2) and V(O5,H) valence basins in the conformer 4. These features can be proven by the bond order analysis and are also in line with the changes of the bond lengths.

BOMD (Born-Oppenheimer Molecular Dynamics) simulations. The formation of a T-shape [NpO_3] intermediate is a critical step in the Path I, therefore the dynamics of this process was simulated using ab initio classical trajectory calculations to obtain a detailed description. Figure 3 illustrates bond length as a function of time for the formation of intermediates 2 (left side of Figure 3) and 3 (right side of Figure 3) from BOMD simulations, and the fluctuation of potential energy is included in supplementary information (ESI, Figure S2).

To start the simulations, the initial structure of trajectories was prepared by perturbing the TS(2,3) conformer slightly into the direction to either reactant or product along the imaginary vibrational mode. As seen in Figure 3, it is clear that the reaction prefers to proceed toward the formation of the intermediate 3 with a T-shape [NpO_3] group, and the coordination bond Np1-O7 is gradually formed in about 200 fs (from 2.4 to 2.1 Å during the simulation), accompanying with the departure of H9 from the hydroxide bond O7-H9. At the same time, hydroxide ion O8-H moves away from the metal Np upon the approach of H9 atom (the distances of Np1-O8 and O8-H9 change from 2.78 to 4.0 Å and 3.2 to 1.4 Å, respectively during the simulation, as shown at the right side of Figure 3). In addition, the potential energy at around 200 fs reveals a decreasing tendency (see Figure S2), suggesting dynamical preference on the formation of intermediate 3. The other coordination bonds (Np1-O4/5/6) remain stable and fluctuate at around 2.3 Å, as expected.

In the case of the formation of the intermediate 2 (left side of Figure 3), there is no proton shift channel and the formation of additional bonds. All bonds do not show much variation, surviving through the whole simulation. Np1-O8 bond tends to be shortened from 2.7(5) to 2.4Å at around 100 fs, and then remains at 2.5Å after 250 fs. Both Np1-O7 bond and O8-H9 distance exhibit the reasonable oscillations in the initial range from 0 to 350 fs.

3.2 Path II via a *cis*-[NpO_2] pathway assisted by water. No matter the activation of the actinyl bonds or the oxo-exchange of the actinyl hydroxide ions, the participation of water is usually indispensable in experiments. According to the mechanism proposed previously for the oxo-exchange of mononuclear uranyl hydroxide, explicit inclusion of a water molecule in the proton shuttle involves the formation of a cis-uranyl intermediate[13, 18, 26]. Although this channel was not looked as a satisfactory explanation in view of energies, the stable cis-uranyl structure does have been successfully synthesized in experiments[26]. To evaluate the importance of such a pathway in the oxo exchange of neptunyl, the formation of cis-neptunyl and its consumption was investigated in terms of structures, energetics, bonding evolution analysis and dynamics simulation.

Structures and Energetics. The corresponding free energy profile is illustrated in Figure 4 with the optimized geometrical parameters of the stationary points and TS. Symmetric and antisymmetric neptunyl stretching frequencies for the stationary points (6 and 7) and imaginary frequencies for transition state TS(6,7) are given in Table 1. Activation enthalpies and Gibbs free energies for the forward (F) and backward (B) processes of Path II are tabulated in Table 2.

In Path II, starting from neptunyl tetrahydroxide and one H_2O molecule, there are two sequential proton shift steps to produce a cis-neptunyl intermediate, i.e. transfer of one proton of water molecule onto axial oxygen of neptunyl at the first step, followed by the migration of another proton of hydroxide ion to recover the deprotonated water molecule. During this process, one axial Np1-O2 bond of neptunyl and one equatorial Np1-O5 bond are elongated (from 1.83 to 2.16 Å) and

shortened (from 2.26 to 1.92 Å) simultaneously, respectively. This finally leads to the formation of a cis-neptunyl conformer to fulfill oxo-ligand exchange.

A barrier of 24.5 kcal/mol was needed to overcome to this pathway, which is only 1.8 kcal/mol higher than that to the rate-determining step of Path I. This suggests that Path II may compete against Path I under appropriate condition. In addition, the energy of the product 7 is much higher than the starting point 6, as shown in Figure 4, implying that the formation of cis-neptunyl is instable due to a strongly endothermic process, and cis-neptunyl hydroxide may evolve back to the linear neptunyl hydroxide with the assistance of water molecule with a backward barrier height of 7.5 kcal/mol. Consequently, the linear neptunyl hydroxide in solution could be a mixture of those produced by oxo-ligand exchange and the intact ones.

Bonding Evolution Analysis. ELF topological analysis of the Path II transverse along XY plane is illustrated in Figure 5 with the geometries of the complexes, in which atoms O4 and O6 are orientated above and below the XY plane, i.e. Z axial direction, while the remaining ones are located closed to the equatorial XY plane. ELF topological map shows that, in the initial complex 6, one H atom of H_2O is close to one axial O atom of neptunyl but without additional disynaptic basin except for Np-O valence basin in neptunyl. The transition state TS(6,7) exhibits a trisynaptic V(O5,H10,O8) basin with H10 atom localization in the middle of O5 and O8, together with a weakened V(O5,H10) basin. The valence Np1-O2 basin in neptunyl is weakened to a great extent accompanying with the emergence of a disynaptic V(O2,H9) basin, as a consequence of Np1-O2 bond breaking. Obviously, during the formation of product 7, one proton firstly shifts from the water to “yl-”oxygen along with the hydroxide O5-H10 bond breaking; subsequently the second proton migrates onto hydroxide ion O8-H. The product 7 possesses two disynaptic basins, i.e. the retained V(Np1-O3) and newly formed V(Np1-O5), while H10 atom previously located in the middle of O5 and O8 fully breaks away from O5 atom and behaves in the bonding region of water, which realized oxo-ligand exchange.

BOMD Simulation. The evolution of potential energy and bond length along with time for the Path II from BOMD simulation are presented in Figure 6. In the initial

point of trajectory, one of axial neptunyl bonds is elongated to 2.0 Å or so and one of equatorial Np-O bonds is shorten to 2.05 Å, while other O and H atoms with hydrogen bond interaction are close to each other at a distance of 1.3 Å or so. The potential energy decreases with the time, implying a strong tendency to form a novel product. From the MD simulation of bond length, it can be noticed that the variation tendency of Np1-O2 and Np1-O5 bonds are opposite, demonstrating the weakening of one axial neptunyl bond and the strengthening of one equatorial bond in around 9fs. Meanwhile, O8-H9 and O5-H10 dehydrogenate to accomplish the proton migration.

As compared to MD simulation of Path I, Path II seems to be considerably rapid (about 8-9 fs) in dynamics. However, their starting points are different, in which the starting point of trajectory in the Path I is close to the transition state with the energy of about 22 kcal/mol relative to the initial complex 1, while one in the Path II is relatively far away from the transition state with the relative energy of 30 kcal/mol more than its initial complex 6. Additionally, the endothermicity of the 1→3 process (about 7.5 kcal/mol) in the Path I is lower than that of 6→7 process (about 17.0 kcal/mol) in the Path II. Accordingly, the Path I is more favored than Path II in the view of reaction barriers and thermodynamics, which agrees with the mechanism proposed in monomeric uranyl hydroxide[9]. Nevertheless, the Path II could take place due to a rapid dynamics process once the higher energy is reached.

3.3 Path III via intramolecular proton transfer in the absence of water. For the sake of complete comparison, we have also taken into account the possible process via the intramolecular proton transfer in the absence of water (see ESI, scheme S1), as previously suggested in oxo exchange of uranyl hydroxide [3, 13]. One pathway (Path III_A) involves the migration of one hydrogen atom directly from equatorial hydroxide ion onto axial neptunyl oxygen, leading to the formation of a bent cis-neptunyl unit, similar to the conformation in the Path II. This process requires a barrier of 38.3 kcal/mol (activation free energy of 38.9 kcal/mol, cf. Table 2.) in our calculation, which is 15 kcal/mol higher than that in the Path II.

Another pathway (Path III_B) concerns a concerted transfer of two hydrogens from

two equatorial hydroxide ions to axial oxygen atoms, respectively, to realize the axial-equatorial oxygen exchange with a very high barrier of 147 kcal/mol. Obviously, these two mechanisms in the Path III cannot provide a reasonable explanation for the experimentally observed process in oxo ligand exchange of neptunyl hydroxide.

3.4 Path IV via intramolecular proton transfer in a binuclear species. Similar to the conclusion proposed in uranyl(VI) hydroxide,[20] in which Moll et al found experimental and theoretical evidence to support the presence of T-shape $[UO_3(OH)_3]^{3-}$ and assumed the binuclear adduct $[UO_2(OH)_4^{2-}\bullet UO_3(OH)_3^{3-}]$ to be the key species for oxo exchange by hydrolysis, structural reorganization, and a rate-dominating step with the proton transfer pathway, both the reaction mechanism and BOMD analysis of Path I suggest that the formation of T-shape $[NpO_3]$ intermediate, i.e. $[NpO_3(OH)_3]^{3-}$, is the most favorable relative to other intermediates in the oxo exchange of neptunyl(VI) hydroxide. Accordingly, it is also possible for neptunyl(VI) hydroxide to form binuclear $[NpO_2(OH)_4^{2-}\bullet NpO_3(OH)_3^{3-}]$ via the interaction between the stable intermediate $[NpO_3(OH)_3]^{3-}$ and the initial reactant $NpO_2(OH)_4^{2-}$. The rate-dominating step for the proton transfer in oxo exchange of binuclear complex is depicted in Scheme 2, in which ΔG and ΔH are also given relative to the dimeric complex 8 for triplet/closed-shell-singlet/open-shell-singlet states at B3LYP/BS1 level with the solvent effect taken into account. As each neptunyl unit carries an unpaired electron, it is possible for the binuclear complex to adopt a triplet, or an open-shell-singlet, or a closed-shell-singlet electronic configuration. Thus, we have investigated the binuclear mechanism in all these three electronic states. Here triplet state is more probable because two single-electrons in the outermost shell are allocated to two metals Np, respectively. In addition, in view of energies, the reactions in the singlet electronic states have too high energy barriers to overcome compared to that in the triplet state (see Scheme 2 in which geometries of triplet dimeric complexes are shown as well).

Scheme 2 shows the proton-transfer reaction 8→9 is feasible due to low activation

barrier (7.9 and 6.6 kcal/mol for $\Delta G^{\ddagger}$ and $\Delta H^{\ddagger}$, respectively), suggesting that once the binuclear complex 8 is formed, oxo exchange reaction can be completed easily. Dimeric complexes 8 and 9 include two T-shape [NpO_3] groups with a Np-O^{yl}-Np bridge, in which complex 8 is formed by the hydrolysis and the structural reorganization of binuclear complex [$NpO_2(OH)_4^{2-}$•$NpO_3(OH)_3^{3-}$]. Entire reaction process keeps two neptunyl planes intersectant. A single imaginary frequency (1203i) of the transition state TS(8,9) describes the proton movement across the energy barrier. The energy difference between the initial binuclear reactant and complex 8 is 24.0 and 15.2 kcal/mol for Gibbs energy and thermal enthalpy, respectively, slightly different from the low energy difference in the case of uranyl(VI)[20]. Therefore, the overall energies to be overcome in the binuclear neptunyl oxo exchange are calculated to be 31.9 and 21.8 kcal/mol for Gibbs energy and thermal enthalpy, respectively relative to the initial binuclear reactant [$NpO_2(OH)_4^{2-}$+ $NpO_2(OH)_4^{2-}$+OH^-], which are higher than in the case of mononuclear neptunyl(VI) oxo exchange (22.7 and 13.1 kcal/mol for $\Delta G^{\ddagger}$ and $\Delta H^{\ddagger}$, respectively), suggesting that the binuclear mechanism can be competitive against the monomeric mechanism Path I only at high temperature. The different compatibility of the binuclear mechanism in the uranyl case and the neptunyl case may be due to the nature of neptunyl(VI) with an unpaired electron which do not favor its dimerization.

4. Conclusion

Oxo-exchange mechanisms of neptunyl(VI) hydroxide in solution were explored in the present calculations. The optimized stationary structures, the reaction paths confirmed by the intrinsic reaction coordinate calculations, and ELF analyses as well as BOMD simulation provide detailed description of the reactions. From the above presented results, the major channel for oxo ligand exchange of mononuclear neptunyl(VI) hydroxide possibly follows a pathway via a T-shape [NpO_3] intermediate involved, similar to that of mononuclear uranyl(VI) hydroxide. In addition, there could be an equilibrium between the four-coordinated neptunyl hydroxide and T-shape complex [$NpO_3(OH)_3 \cdot H_2O]^{3-}$, with a favorable activation

Gibbs energy of 22.7 kcal/mol, which contributes to the occurrence of overall reaction. A potential binuclear mechanism was also investigated, and in the triplet binuclear neptunyl(VI) oxo exchange, once the complex 8 is formed via the interaction between the T-shape $[NpO_3(OH)_3]^{3-}$ and the initial reactant $NpO_2(OH)_4^{2-}$, oxo ligand exchange can be achieved effectively, however, it required a higher overall energy to fulfill the reaction, suggesting a competitive binuclear mechanism against the monomeric mechanism only at high temperature. Both mononuclear and binuclear mechanisms imply that once T-shape $[NpO_3]$ intermediate is formed, it is apt to complete the axial-equatorial oxygen exchange, which is in agreement with the experiment.

The ELF analysis provides a clear descritption for the bonding evolution of Path I and II. In the case of Path I, the ELF values shows the formation of the valence basin V(Np,O7), suggesting the existence of a T-shape $[NpO_3]$ moiety. Combined ab initio molecular dynamics simulations with thermodynamical analysis favors Path I more than Path II. However, the Path II could still take place due to a rapid dynamics process once the higher energy barrier is overcome, indicating that there might be two competitive reaction paths existed for oxo ligand exchange of monomeric neptunyl(VI) hydroxide.

ASSOCIATED CONTENT

Electronic Supplementary Information (ESI) available: the topology analysis for the process 1→3* of Path I, BOMD simulation for the formation of complex 2 and 3 in Path I and Scheme S1 for Path III are available.

AUTHOR INFORMATION

Corresponding Author: *E-mail: dwang@ihep.ac.cn

*E-mail: yangxia@ihep.ac.cn

ACKNOWLEDGMENT

This work was financially supported by the National Natural Science Foundation of China to Z.Chai (No. 91026000),to D.Wang (No. 91226105), and by the Chinese Academy of Sciences in the framework of a Frontier of Novelty program to D.Wang (Nos.Y1515540U1 and Y2291810S3), which are gratefully acknowledged. Calculations were done on the computational grids in the computer center of the Institute of High Energy Physics (IHEP) maintained by Drs. Jingyan Shi and Bowen Kan, in the Supercomputing Center of Chinese Academy of Sciences (SCCAS) and in the National Supercomputing Center in Tianjin (NSCC-TJ).

REFERENCES

1. L. R. Morss, N. M. Edelstein, J. Fuger and J. J. Katz, *The Chemistry of the Actinide and Transactinide Elements*, Springer: Berlin, 2006., 3rd edn.
2. S. Fortier and T. W. Hayton, *Coord. Chem. Rev.* , 2009, 254, 197.
3. D. L. Clark, S. D. Conradson, R. J. Donohoe, D. W. Keogh, D. E. Morris, P. D. Palmer, R. D. Rogers and C. D. Tait, *Inorg. Chem.* , 1999, 38 1456.
4. Ana F. Lucena, Samuel O. Odoh, Jing Zhao, Joaquim Marçalo, Georg Schreckenbach and J. K. Gibson, *Inorg. Chem.*, 2014, 53, 2163.
5. G. Schreckenbach, P. J. Hay and R. L. Martin, *J. Comput. Chem.*, 1999, 20, 70.
6. H. Moll, T. Reich and Z. Szabo, *Radiochim. Acta*, 2000, 88 411.
7. M. Bühl and G. Schreckenbach, *Inorg. Chem.*, 2010, 49, 3821.
8. Z. Szabo and I. Grenthe, *Inorg. Chem.*, 2007, 46, 9372.
9. G. A. Shamov and G. Schreckenbach, *J. Am. Chem. Soc.* , 2008 130 13735.
10. Z. Szabo and I. Grenthe, *Inorg. Chem.* , 2010, 49 4928.
11. S. Tsushima, *Inorg. Chem.* , 2012, 51, 1434.
12. U. Wahlgren, H. Moll, I. Grenthe, B. Schimmelpfennig, L. Maron, V. Vallet and O. Gropen, *J. Phys. Chem. A* 1999, 103, 8257.
13. G. Schreckenbach, P. J. Hay and R. L. Martin, *Inorg. Chem.*, 1998, 37, 4442.
14. S. Tsushima and T. Reich, *Chem. Phys. Lett.*, 2001, 347, 127.
15. I. Infante, B. van Stralen and L. Visscher, *J. Comput. Chem.*, 2006, 27, 1156.
16. K. I. M. Ingram, L. J. L. Häller and N. Kaltsoyannis, *Dalton Trans.*, 2006, 2403.
17. Y. Oda and A. Aoshima, *J. Nucl. Sci. Technol.*, 2002, 39, 647.
18. H. P. Hratchian, J. L. Sonnenberg, P. J. Hay, R. L. Martin, B. E. Bursten and H. B. Schlegel, *J. Phys. Chem. A*, 2005, 109, 8579.
19. D. Rios, M. C. Michelini, A. F. Lucena, J. Marçalo and J. K. Gibson, *J. Am. Chem .Soc.*, 2012, 134, 15488.
20. H. Moll, A. Rossberg, R. Steudtner, B. Drobot, K. Müller and S. Tsushima, *Inorg. Chem.*, 2014, 53, 1585.
21. P. Wahlin, C. Danilo, V. Vallet, F. Réal, J. P. Flament and U. Wahlgren, *J. Chem. Theory Comput.* ,

2008, 4, 569.
22. F. Réal, V. Vallet, U. Wahlgren and I. Grenthe, *J. Am. Chem. Soc.*, 2008, 130, 11742.
23. G. Schreckenbach and G. A. Shamov, *Accounts of Chemical Research*, 2009, 43, 19-29.
24. M. Bühl and G. Wipff, *ChemPhysChem* 2011, 12, 3095.
25. S. J. Harley, C. A. Ohlin, R. L. Johnson, A. F. Panasci and W. H. Casey, *Angew. Chem., Int. Ed.* , 2011, 50, 4467.
26. A. E. Vaughn, C. L. Barnes and P. B. Duval, *Angew. Chem., Int. Ed.* , 2007, 46, 6622.
27. D. L. Clark, S. D. Conradson, R. J. Donohoe, P. L. Gordon, D. W. Keogh, P. D. Palmer, B. L. Scott and C. D. Tait, *Inorg. Chem.*, 2013, 52, 3547-3555.
28. R. G. Parr and W. Yang, in *Density Functional Theory of Atoms and Molecules*, Oxford University Press, New York, 1989.
29. A. D. Becke, *J. Chem. Phys.* , 1993, 98, 5648.
30. P. J. Stephens, C. F. Devlin, M. J. Chabalowski and M. J. Frisch, *J.Phys. Chem.* , 1994, 98, 11623.
31. F. Réal, V. Vallet, U. Wahlgren and I. Grenthe, *Journal of the American Chemical Society*, 2008, 130, 11742-11751.
32. F. Schlosser, S. Krüger and N. Rösch, *Inorganic Chemistry*, 2006, 45, 1480-1490.
33. T. Yang and B. E. Bursten, *Inorganic Chemistry*, 2006, 45, 5291-5301.
34. G. Schreckenbach, P. J. Hay and R. L. Martin, *J. Comput. Chem.* , 1999, 20, 70.
35. N. Kaltsoyannis, *Chem. Soc. Rev.*, 2003, 32, 9.
36. N. Kaltsoyannis, P. J. Hay, J. Li, J.-P. Blaudeau and B. E. Bursten, in *The Chemistry of The Actinide and Transactinide Elements*, eds. L. R. Morss, N. M. Edelstein, J. Fuger and J. J. Katz, Springer: Dordrecht. The Netherlands, 2008, pp. p1893-2012.
37. J.-H. Lan, W.-Q. Shi, L.-Y. Yuan, J. Li, Y.-L. Zhao and Z.-F. Chai, *Coord. Chem. Rev.* , 2012, 256, 1406.
38. D. Wang, W. F. van Gunsteren and Z. Chai, *Chem. Soc. Rev.* , 2012, 41, 5836.
39. X. Y. Cao, M. Dolg and H. Stoll, *J. Chem. Phys.*, 2003, 118, 487.
40. W. Küchle, M. Dolg, H. Stoll and H. Preuss, *The Journal of chemical physics*, 1994, 100, 7535.
41. P. C. Hariharan and J. A. Pople, *Theor. Chim. Acta* 1973, 28, 213.
42. D. Rios, M. C. Michelini, A. F. Lucena, J. Marçalo, T. H. Bray and J. K. Gibson, *Inorganic Chemistry*, 2012, 51, 6603-6614.
43. M. d. C. Michelini, N. Russo and E. Sicilia, *J. AM. CHEM. SOC.* , 2007, 129, 4229.
44. V. Barone, M. Cossi and J. Tomasi, *J. Comput. Chem.* , 1998, 19, 404.
45. C. Gonzalez and H. B. Schlegel, *J. Chem. Phys.* , 1989, 90, 2154.
46. C. Gonzalez and H. B. Schlegel, *J. Phys. Chem. A*, 1990, 94, 5523.
47. M. J. Frisch, G. W. Trucks, H. B. Schlegel, G. E. Scuseria, M. A. Robb, J. R. Cheeseman, G. Scalmani, V. Barone, B. Mennucci, G. A. Petersson, H. Nakatsuji, M. Caricato, X. Li, H. P. Hratchian, A. F. Izmaylov, J. Bloino, G. Zheng, J. L. Sonnenberg, M. Hada, M. Ehara, K. Toyota, R. Fukuda, J. Hasegawa, M. Ishida, T. Nakajima, Y. Honda, O. Kitao, H. Nakai, T. Vreven, J. A. Montgomery, J. E. Peralta, F. Ogliaro, M. Bearpark, J. J. Heyd, E. Brothers, K. N. Kudin, V. N. Staroverov, R. Kobayashi, J. Normand, K. Raghavachari, A. Rendell, J. C. Burant, S. S. Iyengar, J. Tomasi, M. Cossi, N. Rega, J. M. Millam, M. Klene, J. E. Knox, J. B. Cross, V. Bakken, C. Adamo, J. Jaramillo, R. Gomperts, R. E. Stratmann, O. Yazyev, A. J. Austin, R. Cammi, C. Pomelli, J. W. Ochterski, R. L. Martin, K. Morokuma, V. G. Zakrzewski, G. A. Voth, P. Salvador, J. J. Dannenberg, S. Dapprich, A. D. Daniels, Ö. Farkas, J. B. Foresman, J. V. Ortiz, J. Cioslowski and

D. J. Fox, GAUSSIAN 09, Gaussian, Inc., Wallingford, CT, 2009.

48. V. Bakken, J. M. Millam and H. B. Schlegel, *J. Chem. Phys.* , 1999, 111, 8773.
49. J. M. Millam, V. Bakken, W. Chen, W. L. Hase and H. B. Schlegel, *J. Chem. Phys.* , 1999, 111, 3800.
50. A. Savin, R. Nesper, S. Wengert and T. F. Fässler, *Angewandte Chemie International Edition in English*, 1997, 36, 1808-1832.
51. B. Silvi and A. Savin, *Nature*, 1994, 371, 683-686.
52. T. Lu and F. Chen, *J. Comp. Chem.* , 2012, 33, 580.
53. I. Mayer, *Int. J. Quantum Chem.* , 1984, 26, 151.
54. K. B. Wiberg, *Tetrahedron*, 1968, 1083.

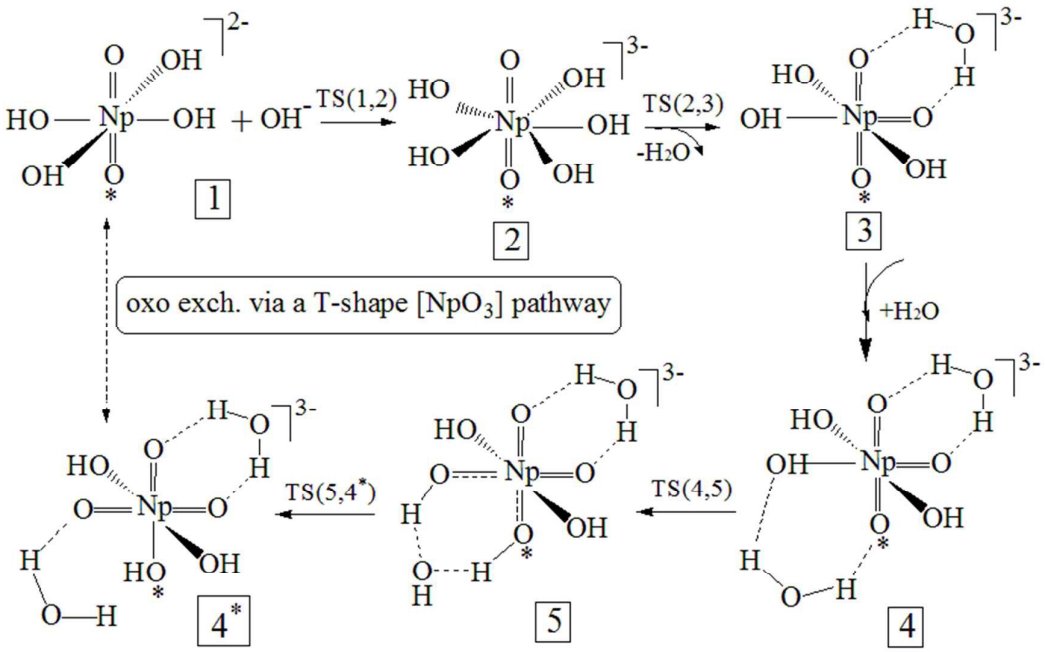

Scheme 1. The 'yl-'Oxygen Exchange of Neptunyl Hydroxide via a T-shape [NpO_3] pathway. The "O*" represents the O^{yl} atom that is to be exchanged.

Table 1.Calculated Bond Distances (Å), Angles (deg), Neptunyl Stretching Frequencies (Symmetric $v_{sym.}$, Antisymmetirc$v_{asym.}$, cm^{-1}) of Different Species, and Imaginary Frequencies (v_i) of Transition States Fully Optimized in the Aqueous Phase at B3LYP/BS1 Level.

Species[a]	Np=O	O=Np=O	Np-OH	Np-O-H	O=Np-OH	$v_{sym.}$ [b]	$v_{asym.}$ [b]	v_i [c]
1	1.81 (1.79-1.82)[d]	180.0 (180.0)[d]	2.27 (2.24)[d]	114.8-115.1	89.2-90.7 (90.2)[d]	752 (769)[d]	803	
2	1.82	176.7	2.34-2.48	93.9-111.7	88.5-92.2	730	784	
3	1.86,1.87,2.02	175.4, 93.7, 90.9	2.32-2.35	110.0-113.4	87.6-92.1, 178.4	708	702	
4	1.86,1.86,2.00	175.7, 93.9, 90.4	2.31-2.39	110.3-114.1	87.9-92.8, 177.5	712	707	
5	1.91, 1.91	92.4	2.13-2.30, 3.80	110.4-114.1	88.5-91.5, 175.6	702	597	
6	1.81, 1.83	179.3	2.26	115.2-119.6	87.7-90.6	752(trans-)	804(trans-)	
7	1.87, 1.92	96.9	2.16-2.26	114.5-117.9	88.3-92.8, 174.3	731(cis-)	648(cis-)	
TS(1,2)	1.82	176.9	2.34-2.47	93.9-110.9	88.8-91.8	734	786	68i
TS(2,3)	1.82	178.5	2.28-2.73	92.8-113.6	88.9-91.4	727	779	66i
TS(3,3*)	1.93, 2.08	168.4,98.5, 93.1, 69.9	2.34,	113.7, 114.4	89.1-90.9	704	578, 641	1767i
TS(4,5)	1.89,1.93,2.06	175.6, 92.7, 91.6	2.18, 2.30, 3.78	108.2-117.8	84.9-91.4, 177.5	700, 547	609	227i
TS(6,7)	1.83, 2.05, 2.05	95.8	2.05-2.24	111.8-118.3	84.6-90.9, 179.6	775, 617	730	756i

[a] **1**=$[NpO_2(OH)_4]^{2-}$, **2** = $[NpO_2(OH)_5]^{3-}$, **3**=$[NpO_3(OH)_3\cdot H_2O]^{3-}$, **4** = $[NpO_3(OH)_3\cdot 2H_2O]^{3-}$, **5**=*cis*-$[NpO_2(OH)_5\cdot H_2O]^{3-}$, **6**=$[NpO_2(OH)_4\cdot H_2O]^{2-}$, **7**=*cis*-$[NpO_2(OH)_4\cdot H_2O]^{2-}$. The symbol "*" refers to oxo ligand exchange occurred. [b] data in parentheses are experimental values from Ref. [26].

Table 2. The thermicity (kcal/mol) of the Forward (F) and Backward (B) Reactions for Paths I, II and III in the aqueous phase[a,b]

Path I	$\Delta H^{\ddagger F}$	$\Delta H^{\ddagger B}$	ΔH_{298}	$\Delta G^{\ddagger F}$	$\Delta G^{\ddagger B}$	ΔG_{298}	$\Delta E^{\ddagger F}$ [b]	$\Delta E^{\ddagger B}$ [b]
(1→2)	13.1(12.5)[c]	0.6(9.5)[c]	12.5 (3.0)[c]	22.7(21.3)[c]	0.6(8.0)[c]	22.1 (13.3)[c]	8.1	0.2
(2→3)	0.3 (1.0)[d]	11.4 (15.2)[d]	-11.1(-14.2)[d]	0.9(1.6)[d]	14.1(16.6)[d]	-13.2 (-14.9)[d]	0.4	6.8
(3→3*)	27.6(14.5)[d]	27.6 (14.5)[d]	0.0(0.0)[d]	29.3(15.5)[d]	29.3(15.5)[d]	0.0(0.0)[d]	42.4	42.4
(4→5) [e]	9.2	0.2	9.0	12.4	0.2	12.2	14.3	0.8
(5→4*)	0.2	9.2	-9.0	0.2	12.4	-12.2	0.8	14.3
Path II	$\Delta H^{\ddagger F}$	$\Delta H^{\ddagger B}$	ΔH_{298}	$\Delta G^{\ddagger F}$	$\Delta G^{\ddagger B}$	ΔG_{298}	$\Delta E^{\ddagger F}$ [b]	$\Delta E^{\ddagger B}$ [b]
(6→7)	22.6(15.5)[d]	5.5 (4.5)[d]	17.1 (11.0)[d]	24.5(15.6)[d]	7.5(4.7)[d]	17.0 (10.8)[d]	40.3	12.4
Path III	$\Delta H^{\ddagger F}$	$\Delta H^{\ddagger B}$	ΔH_{298}	$\Delta G^{\ddagger F}$	$\Delta G^{\ddagger B}$	ΔG_{298}	$\Delta E^{\ddagger F}$ [b]	$\Delta E^{\ddagger B}$ [b]
III_A	38.3(37.5)[f]	20.6	17.8	38.9	21.6	17.3	62.8	37.7
III_B	147.1(58.6)[f]	147.1	0.0	146.6	146.6	0.0	125.5	125.5

[a] ΔH_{298} and ΔG_{298} correspond to the overall enthalpy change and the free energy change of a reaction at B3LYP/BS1 level. [b] ΔE corresponds to the single point calculation at MP2/BS2 level. [c] values in the parentheses is from ref.9, corresponding to oxo ligand exchange of uranyl hydroxide calculated at PBE level in solution. [d] values in the parentheses is in gas phase from ref.9. [e] no intermediate was found for oxo ligand exchange of uranyl hydroxide at the process 4→4* in ref.9, where $\Delta G^{\ddagger F}$, $\Delta G^{\ddagger B}$ and ΔG_{298} correspond to 5.7, 5.7 and 0.0 kcal/mol, respectively in solution. [f] cf. ref.12 for oxo ligand exchange of uranyl hydroxide.

Table 3. Valence Basin Population (in electrons) and Bond Order Analysis for Species Involved in Path I, Calculated at the B3LYP/BS1 Level.[a]

Species		(1→2)			(2→3)		(3→3*)			(4→5)			(5→4*)	
		1	TS(1,2)	2	TS(2,3)	3	TS(3,3*)	3*	4	TS(4,5)	5	TS(5,4*)	4*
valence basin population[b]	V(Np,O2)	1.90	1.88	1.89	1.84	1.80	1.68	1.36	1.80	1.57	1.53	1.51	1.35
	V(Np,O3)	1.90	1.88	1.89	1.88	1.81	1.72	1.71	1.82	1.73	1.67	1.71	1.72
	V(Np,O5)	1.22	1.14	1.13	1.19	1.22	1.46	1.79	1.27	1.55	1.60	1.65	1.79
	V(Np,O7)	1.23	1.12	1.20	1.42	1.71	1.73	1.80	1.72	1.69	1.71	1.73	1.80
bond order[c]	Np-O2	1.40	1.23	1.21	1.13	1.21	0.90	0.47	1.20	0.70	0.64	0.58	0.50
		(2.85)	(2.84)	(2.84)	(2.83)	(2.72)	(1.82)	(1.08)	(2.65)	(1.79)	(1.56)	(1.19)	(1.10)
	Np-O3	1.39	1.22	1.20	1.12	1.22	1.17	0.94	1.20	1.12	1.07	1.02	0.98
		(2.85)	(2.84)	(2.84)	(2.83)	(2.66)	(2.48)	(2.18)	(2.68)	(2.62)	(2.58)	(2.50)	(2.22)
	Np-O5	0.55	0.55	0.53	0.49	0.57	0.90	1.21	0.52	0.62	0.63	0.98	1.21
		(1.16)	(1.00)	(1.00)	(0.93)	(1.08)	(1.82)	(2.71)	(1.04)	(1.39)	(1.54)	(2.22)	(2.74)
	Np-O7	0.57	0.50	0.56	0.55	0.95	1.17	1.21	0.94	1.02	1.07	1.12	1.23
		(1.17)	(0.88)	(1.03)	(1.05)	(2.18)	(2.49)	(2.71)	(2.15)	(2.50)	(2.58)	(2.62)	(2.68)

[a] The sequence numbers of atoms are same as in Figure 1. Those Np-O bonds with main alteration are selected here. [b] valence basins generally do not include a nucleus. [c] Mayer bond order and Wiberg bond index (in parentheses).

Figures Captions:

Scheme 1. The 'yl-'Oxygen Exchange of Neptunyl Hydroxide via a T-shape [NpO_3] pathway. The "O*" represents the O^{yl} atom that is to be exchanged.

Figure 1. Calculated relative free energy (kcal/mol) for Path I via the T-shape [NpO_3] pathway at B3LYP/6-311++G(d,p) level combined with small core RECP in the aqueous phase.

Figure 2. ELF shaded surface map with projection (on left) and contour line map (on middle) of stationary points involving in the reaction pathway $4 \rightarrow 4^*$. The corresponding structures with the direction of the Cartesian axis are shown on the right-hand side.

Figure 3. Bond length as a function of time evolution towards the formation of complexes 2 (left side) and 3 (right side) from BOMD simulation.

Figure 4. Calculated relative free energy (kcal/mol) for Path II via a cis-neptunyl structure assisted by a water molecule at B3LYP/6-311++G(d,p) level combined with small core RECP in the aqueous phase.

Figure 5. ELF shaded surface map with projection (left side) and contour line map (middle) of stationary points in XY plane on Path II, with inclusion of optimized conformations orientated in the coordinate axis (right side).

Figure 6. Potential energy (upper) and bond length (lower) along with time evolution towards the formation of product 7 on the Path II from BOMD simulation.

Scheme 2. Binuclear neptunyl(VI) oxo exchange and Gibbs energy change and enthalpy change calculated at B3LYP/BS1 level. Energies are in kcal/mol for triplet/closed-shell-singlet/open-shell-singlet states. The "O*" represents the O^{yl} atom that is to be exchanged.

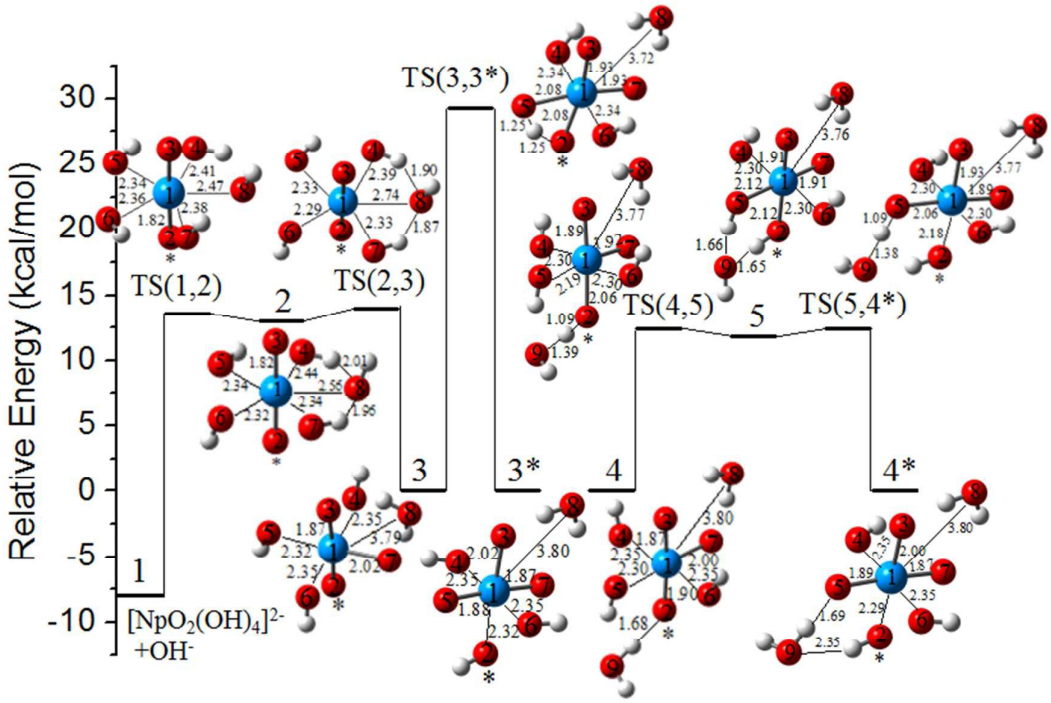

Figure 1.

Path I_4→4*

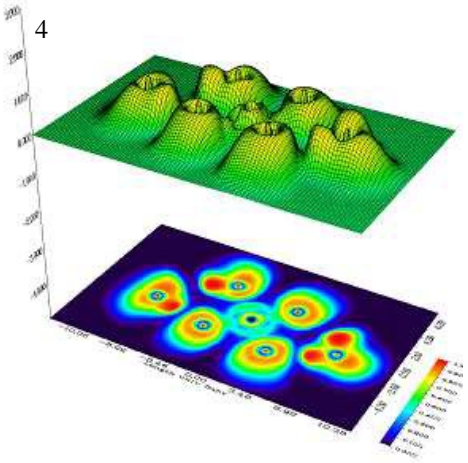

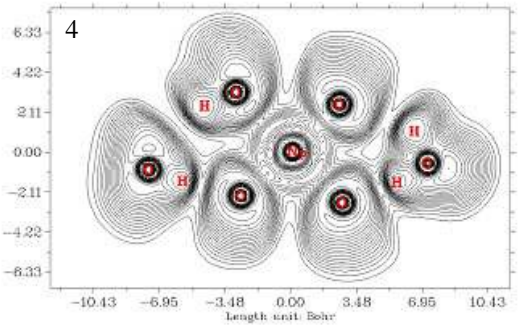

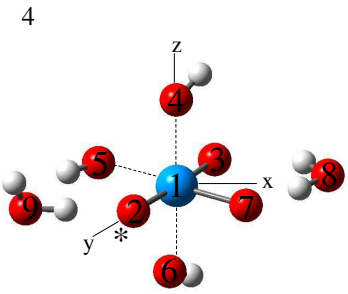

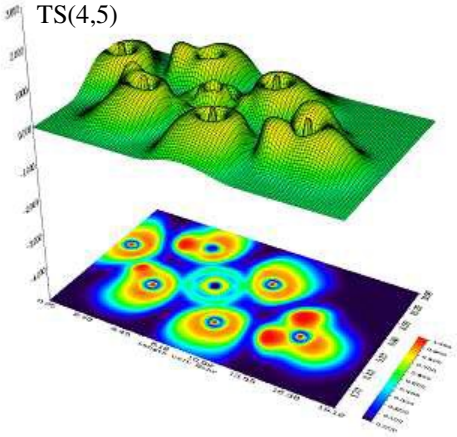

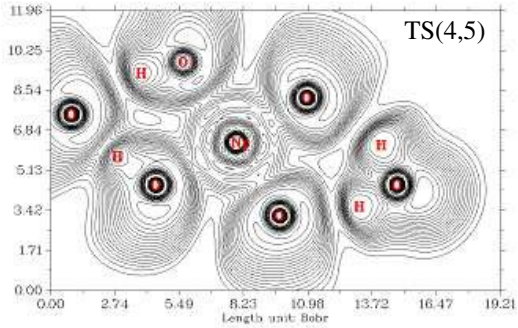

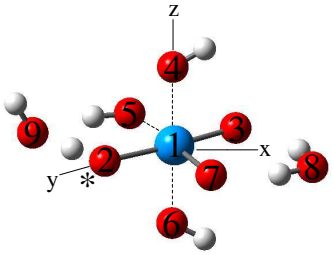

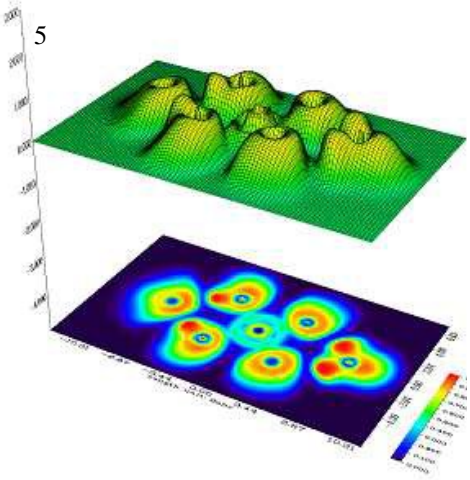

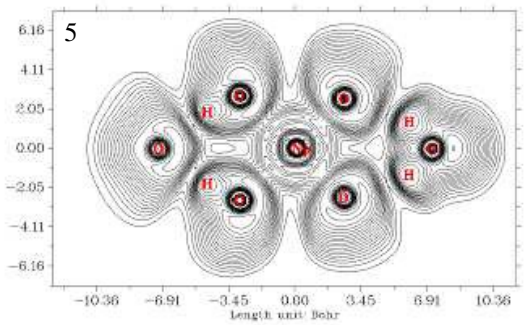

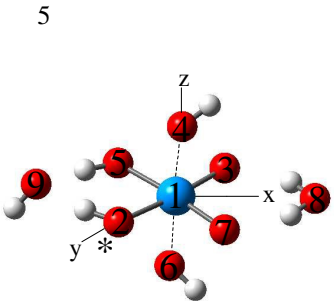

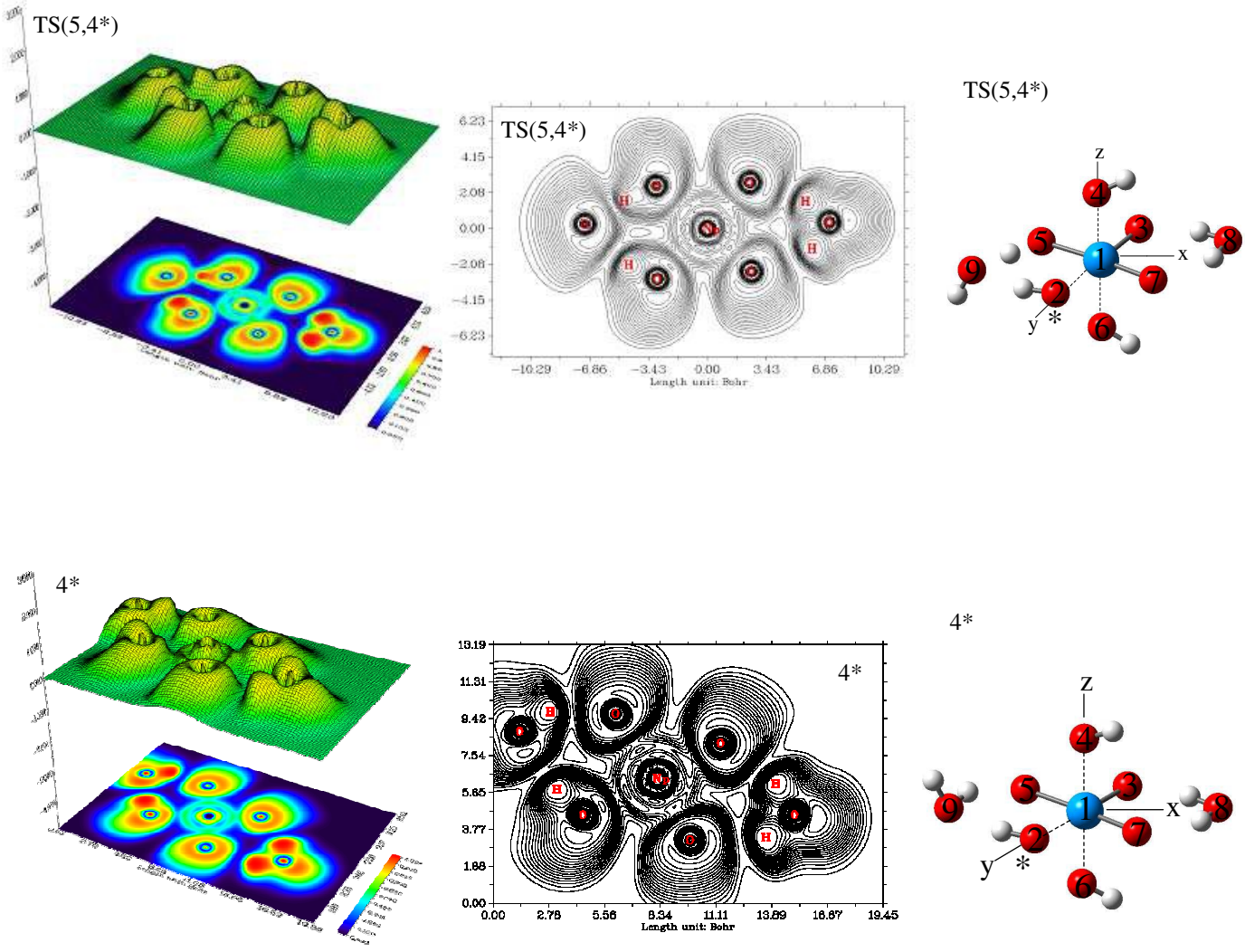

Figure 2.

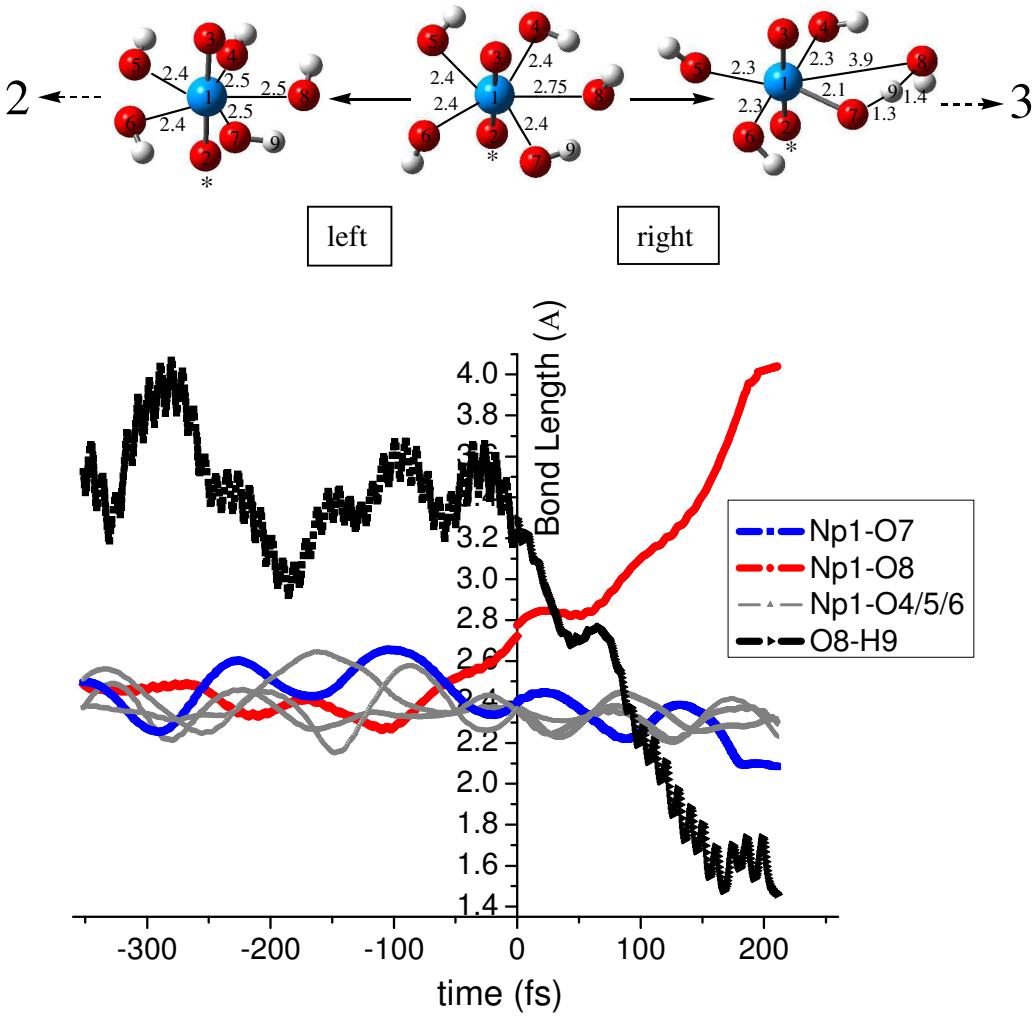

Figure 3.

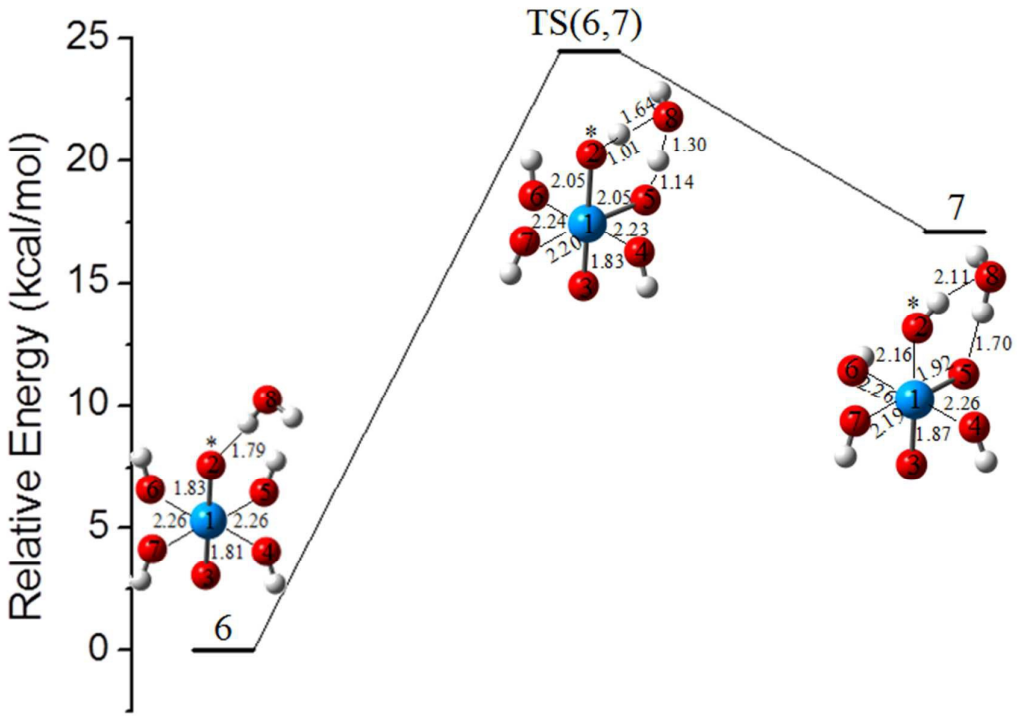

Figure 4.

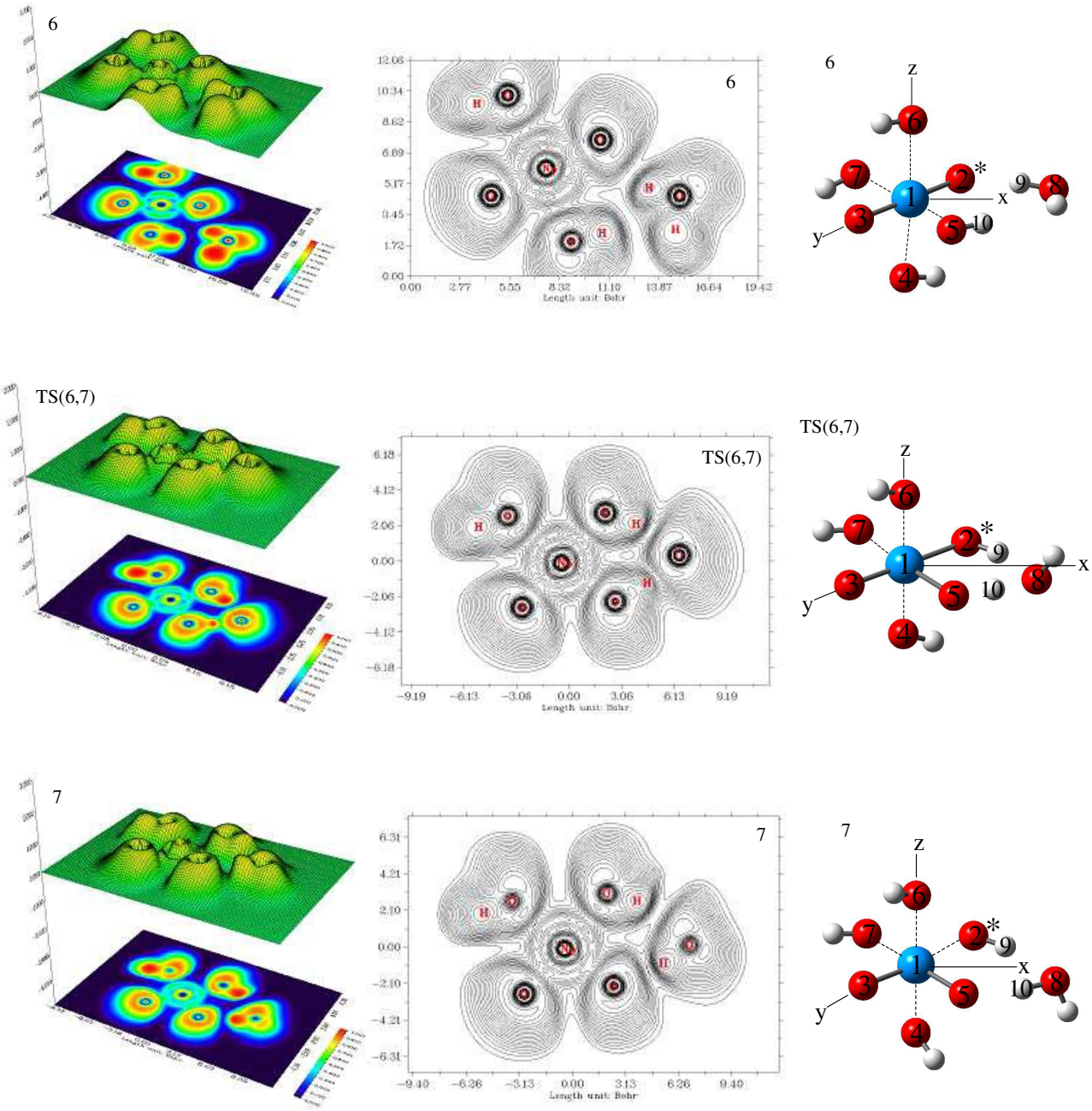

Figure 5.

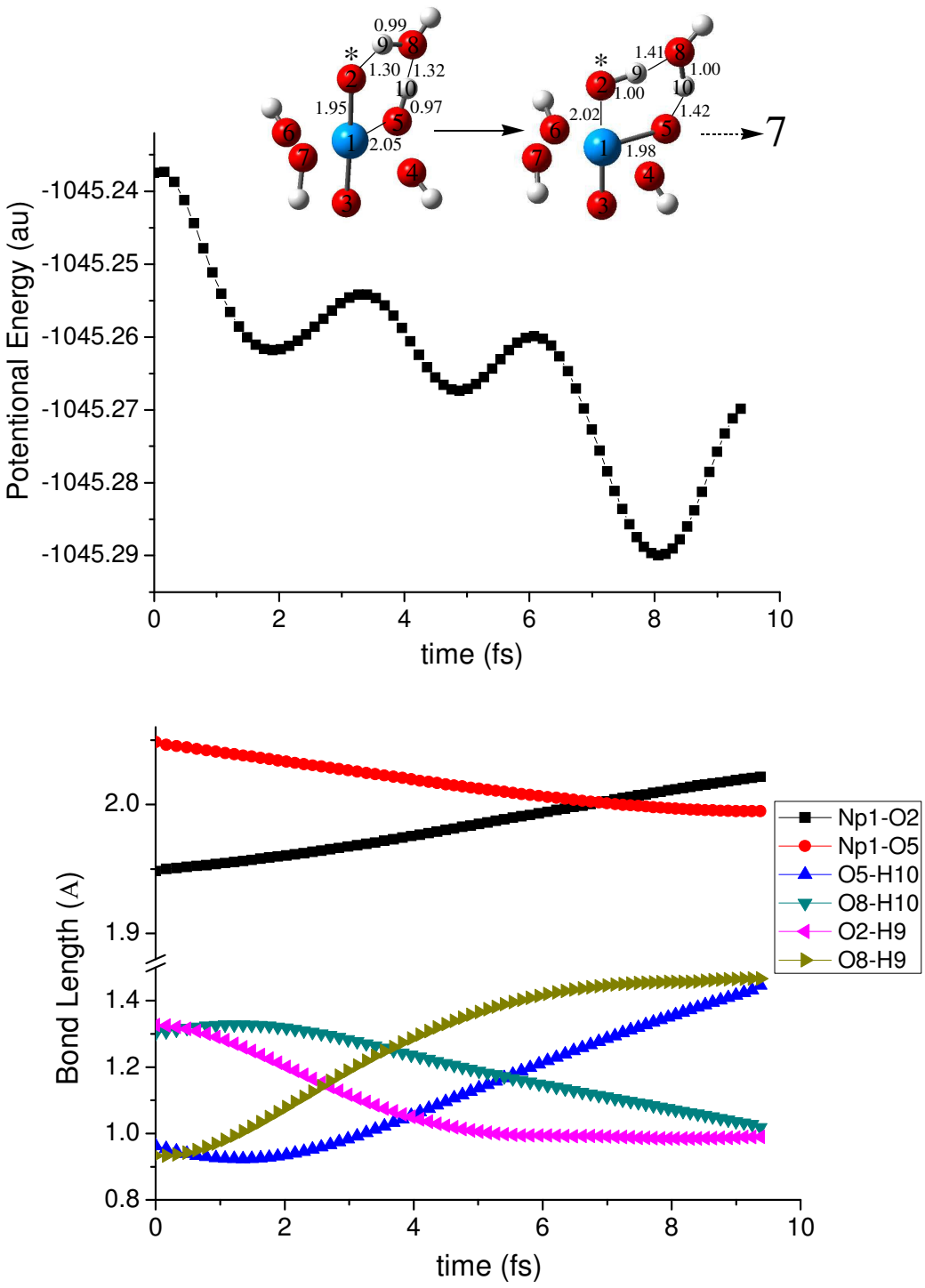

Figure 6.

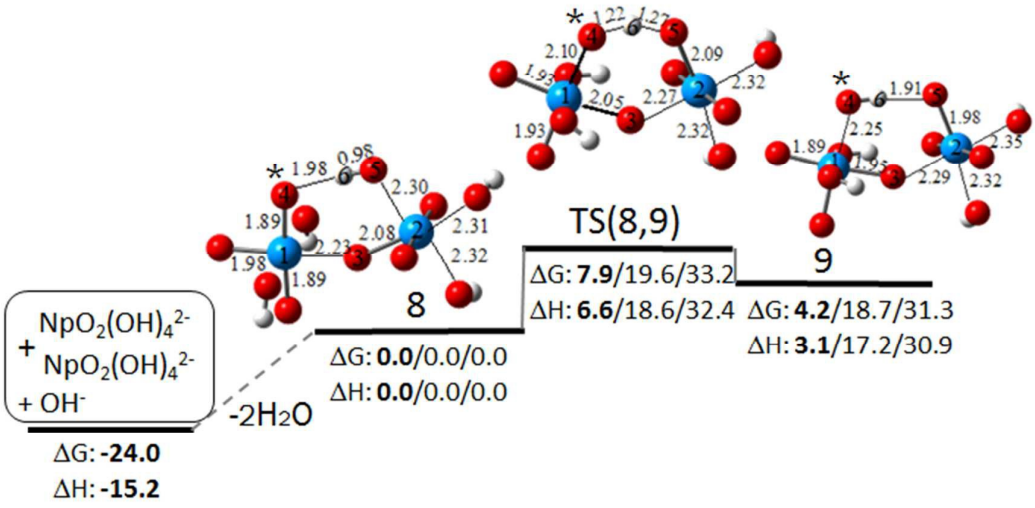

Scheme 2. Binuclear neptunyl(VI) oxo exchange and Gibbs energy change and enthalpy change calculated at B3LYP/BS1 level. Energies are in kcal/mol for triplet/closed-shell-singlet/open-shell-singlet states. The "O*" represents the O^{yl} atom that is to be exchanged.

TOC:

Oxo-exchange of neptunyl(VI) hydroxide: three possible mechanisms.